

# Pressure-Modulated Luminescence Enhancement and Quenching in a Hydrogen-Bonded Organic Framework

Sicheng Wang, Peter E. VanNatta, Bin Wang, Zhenxian Liu, Abdullah M. Al-Enizi, Ayman Nafady, Shengqian Ma,\* and Hao Yan\*

Light emission in the solid state is central for illumination, sensing, and imaging applications. Unlike luminescence in dilute solutions, where the excited states are unimolecular in nature, intermolecular interaction plays a significant role in the quantum yield of solid-state luminophores, manifested as competing aggregation-caused quenching (ACQ) and aggregation-induced enhancement (AIE). Both effects are extensively studied in various systems; however, it remains unclear how their competition depends on molecular conformation and intermolecular stacking. Here the direct observation of pressure-modulated AIE-ACQ competition in a crystalline hydrogen-bonded organic framework (HOF) is reported. Using in situ spectroscopies and computational modeling, the intramolecular vibration and intermolecular  $\pi$ - $\pi$  stacking directly responsible for the non-radiative decay of the excited state are identified. The extent of these two contributions is modulated by hydrostatic pressure and guest molecules in the HOF pores. This work demonstrates a physically neat model system to understand and control solid-state luminescence, and a potential material platform for piezoluminescent sensing.

luminophore in the solid state suppresses the former, leading to aggregation-induced enhancement (AIE), while enhancing the latter, giving rise to aggregation-caused quenching (ACQ).<sup>[2]</sup> Both effects have been individually investigated in different compounds.<sup>[3]</sup> Fluorescent quenching by aggregation has long been documented in molecular fluorophores in both solution<sup>[4,5]</sup> and solid phase,<sup>[6]</sup> as well as conjugated polymers<sup>[7,8]</sup> and quantum dots.<sup>[9]</sup> Particularly, in systems with extended conjugations, diffusion of the excited state through  $\pi$ - $\pi$  stacking has been found to be a major contribution to ACQ.<sup>[10]</sup> On the other hand, Tang et al. first coined the terms AIE and AIEgen to refer to systems where aggregation suppresses non-radiative decay of the excited state.<sup>[2,11]</sup> Such systems usually feature low-frequency vibrational modes that couple with the excited states; aggregation enhances emission by suppressing the vibronic coupling. The AIE effect has been demonstrated

## 1. Introduction

The photoluminescence (PL) quantum yield of solid-state molecular luminophores is significantly affected by two non-radiative decay pathways, namely the vibronic coupling between the excited state and molecular vibrations, and the through-space diffusion of the excited state.<sup>[1]</sup> Aggregation of the

in 1-methyl-1,2,3,4,5-pentaphenylsilole,<sup>[11]</sup> tetraphenylethene (TPE) derivatives,<sup>[12]</sup> and cyclooctatetrathiophene (COTh).<sup>[13]</sup> Apart from the enhanced luminescence brightness, these systems have also found applications in chemical and biological analyses,<sup>[14,15]</sup> immunoassay,<sup>[16]</sup> environment monitoring,<sup>[17]</sup> and food safety.<sup>[18]</sup> In principle, both AIE and ACQ can be present in a luminophore, with the net effect depending on the competition between the two. Understanding and controlling such competition is instrumental for the design of energy-efficient solid-state luminescent materials. However, most model systems investigated to date only manifest one of the two effects, while falling short of revealing the underlying mechanism for their competition.

Mechanical pressure provides a powerful tool to study the effect of intra- and inter-molecular interactions on optical properties. Using hydrostatic pressure generated, for example, in a diamond anvil cell (DAC), the molecular conformation and crystal packing can be continuously and quasi-statically changed without altering the chemical composition. These changes can be tracked using in situ spectroscopies. Zou et al. reported the pressure-induced emission enhancement (PIEE),<sup>[19]</sup> where pressure effectively suppresses intramolecular vibronic couplings and enhances the PL efficiency. More recently, Zou, Fang, and coworkers reported opposite AIE and

S. Wang, P. E. VanNatta, B. Wang, S. Ma, H. Yan  
Department of Chemistry  
University of North Texas  
Denton, TX 76205, USA  
E-mail: [Shengqian.Ma@unt.edu](mailto:Shengqian.Ma@unt.edu); [Hao.Yan@unt.edu](mailto:Hao.Yan@unt.edu)

Z. Liu  
Department of Physics  
University of Illinois Chicago  
Chicago, IL 60607, USA

A. M. Al-Enizi, A. Nafady  
Department of Chemistry  
College of Science  
King Saud University  
Riyadh 11451, Saudi Arabia

The ORCID identification number(s) for the author(s) of this article can be found under <https://doi.org/10.1002/sml.202411362>

DOI: 10.1002/sml.202411362

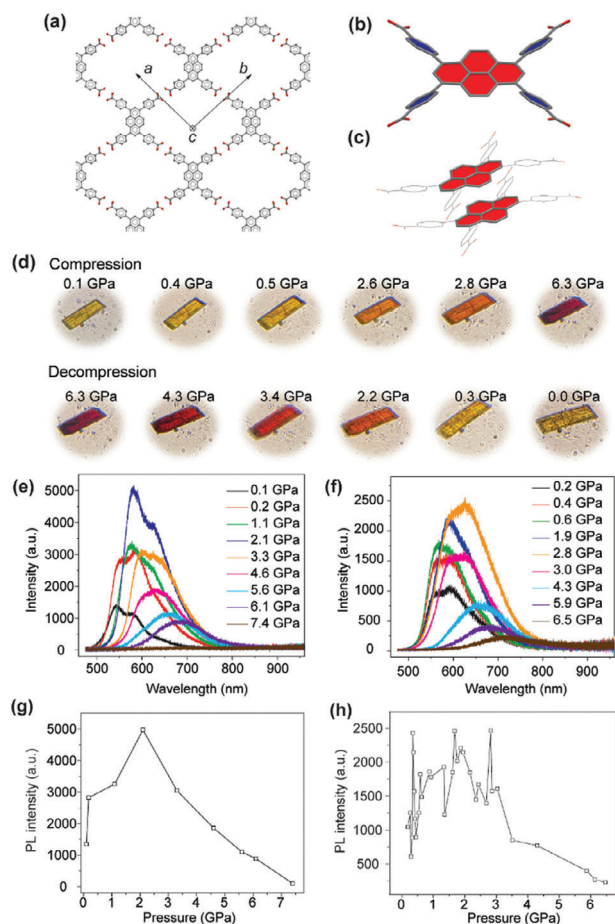


**Figure 1.** a) Structures of PFC-1 at ambient pressure. Carbon, oxygen, and hydrogen atoms are represented by grey, red, and white sticks, respectively. b) The orientation of the phenyl side groups (blue) relative to the pyrene plane (red). c) Interlayer stacking along the *c*-axis. Hydrogen atoms are omitted in (b,c) for clarity. d) Optical micrographs of a PFC-1 crystal along the compression-decompression series. e,f) PL spectra of PFC-1 at different pressures with silicone oil (e) and neon (f) as the PTM. Excitation wavelength: 473 nm. g,h) Peak PL intensity versus pressure for (e,f).

ACQ effects in the isorecticular covalent organic frameworks (COFs) JUC-635 and 636.<sup>[20]</sup> A solid-state luminophore showing pressure-modulated competing ACQ and AIE would be an ideal platform to investigate the factors determining the dominant effect. However, the pressure-modulated crossover between AIE and ACQ in a single system has not been observed to date.

## 2. Results and Discussion

Here we report the experimental observation of competing AIE and ACQ under pressure. Our model system is a hydrogen-bonded organic framework (HOF), namely PFC-1,<sup>[21]</sup> consisting of 1,3,6,8-tetra(4'-carboxyphenyl)pyrene ( $H_4$ TBAPy) interconnected by hydrogen-bonded carboxylic groups into a 3D porous crystalline framework with *sql* topology (Figure 1a; Figure S1, Supporting Information). The dihedral angles between the phenyl side groups and the pyrene plane

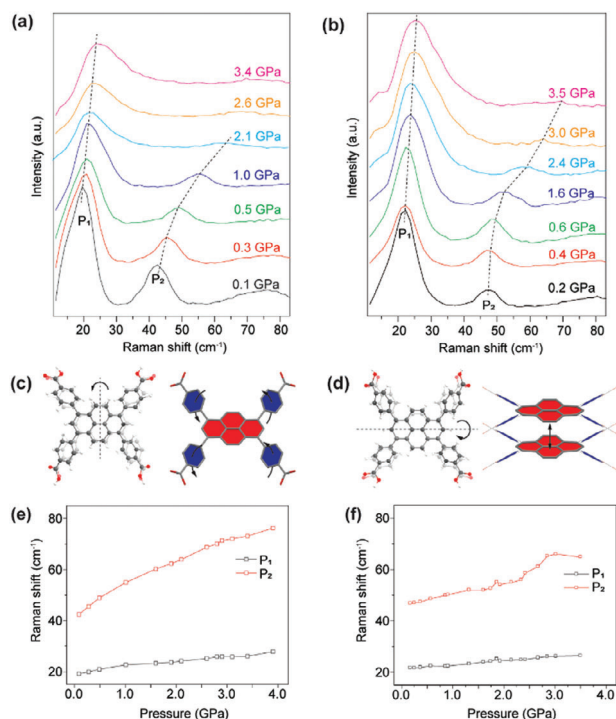


**Figure 2.** a,b) Pressure-dependent Raman spectra of PFC-1 in silicone oil (a) and neon (b). Excitation wavelength: 785 nm. c,d) Atom displacement (left) and schematic of the principal motion (right) associated with  $P_1$  (c) and  $P_2$  (d). e,f) Raman shifts of  $P_1$  and  $P_2$  versus pressure in silicone oil (e) and neon (f).

range from  $38.5^\circ$  to  $42.3^\circ$  (Figure 1b). The nonplanarity, dubbed a “twisted structure” motif,<sup>[22]</sup> is enforced by the orientation of the hydrogen bonding network and may suppress ACQ at ambient pressure.<sup>[23]</sup> The pyrene planes stack along the *c*-axis in a nearly normal orientation relative to the  $H_4$ TBAPy plane, with a perpendicular interlayer distance of  $3.338 \text{ \AA}$  at ambient pressure (Figure 1c). This well-aligned stacking of the  $\pi$ -system is characteristic of molecular luminophores that exhibit ACQ in the solid-state.<sup>[24]</sup> Lastly, the crystal structure features 1D square channels of  $\approx 19 \times 19 \text{ \AA}^2$  cross sections (Figure 1a), which grant exogenous molecules access to the interior of the crystal.

### 2.1. Pressure-Modulated PL in PFC-1

We hypothesize that pressure changes both the intra- and intermolecular interactions, thereby modulating AIE and ACQ. Single crystals of PFC-1 exhibit piezochromism under hydrostatic pressure using silicone oil as the pressure-transducing medium (PTM). As pressure increases from 0.1 to 6.3 GPa, the color evolves from yellow to orange and eventually red. This change is fully reversible upon release of pressure (Figure 1d). The Raman modes show a universal blueshift with increasing pressure, consistent with pressure-induced bond stiffening (Figure S2, Supporting Information). Both the Raman and PL spectrum are fully reversible upon releasing the pressure (Figures S2 and S3, Supporting Information), indicating intactness of the crystal structure during compression. PL spectra of PFC-1 in silicone

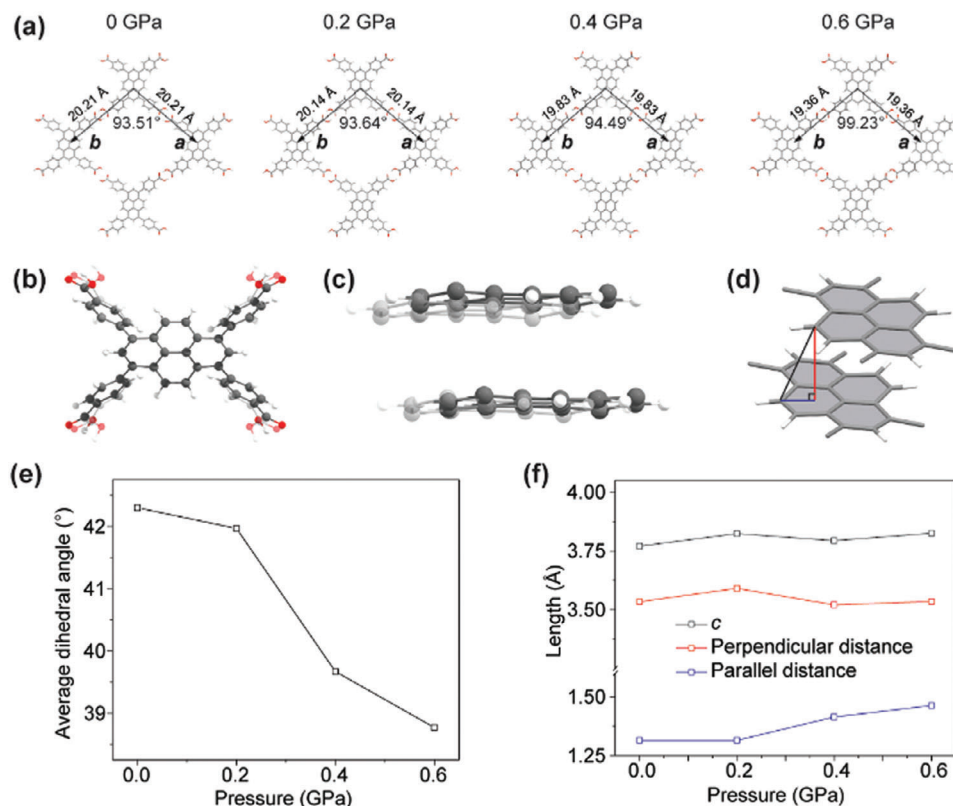


**Figure 3.** a) DFT-computed structures of PFC-1 at 0, 0.2, 0.4 and 0.6 GPa. b) Overlaid  $H_4TBAPy$  at 0 (solid) and 0.6 (semi-transparent) GPa. The molecules are rotated and translated such that the pyrenes overlap. c) Overlaid  $\pi$ -stacked  $H_4TBAPy$  at 0 (solid) and 0.6 (semi-transparent) GPa, viewed perpendicular to the  $c$ -axis. The side groups are omitted to highlight the pyrene interlayer distances. d) Schematic showing the definition of the perpendicular (red) and parallel (blue) interlayer distances. The red and blue lines are perpendicular and parallel to the pyrene plane, respectively. e) Average pyrene-phenyl dihedral angle versus pressure. f) Parallel distance, perpendicular distance, and length of  $c$ -axis versus pressure.

oil at ambient pressure (black, Figure 1e) reveal two peaks at 530 and 570 nm. A similar feature has been observed in PFC-1 dry powders and  $H_4TBAPy$  powders suspended in water.<sup>[25,26]</sup> The exact origins of the two peaks are unknown. In aggregated perylene, the similar two PL peaks at 570 and 600 nm are attributed to emission from shallow (“Y state”) and deep (“E state”) self-trapped excitons.<sup>[27]</sup> Regardless, the PL peaks observed here are clearly excimeric in nature, as the monomer emission of  $H_4TBAPy$  occurs at a shorter,  $\approx 450$  nm, wavelength.<sup>[25,26,28]</sup> Crystal in silicone oil as the PTM induces a constant redshift of the main peak from 543 nm at 0.1 GPa to 690 nm at 6.1 GPa (Figure 1e). The intensity of PL increases by a factor of 270% from 0.1 to 2.1 GPa, then decreases to 65% at 6.1 GPa and vanishes at 7.4 GPa (Figure 1g). This bimodal change of the PL intensity is indicative of competing emission enhancement and quenching mechanisms under pressure. A similar phenomenon is observed when neon gas is used as the PTM: The main peak redshifts from 562 nm at 0.2 GPa to 705 nm at 6.5 GPa (Figure 1f); The PL intensity increases by a factor of 242% from 0.2 to 2.8 GPa before decreasing to 37% by 6.5 GPa (Figure 1h). Notably, the crossover from PL enhancement to suppression occurs at a higher pressure in neon than in silicone oil, suggesting that the molecular-level HOF-PTM interaction plays an important role.

## 2.2. Raman Spectroscopy

In solid-state fluorophores, luminescence enhancement and quenching are related to suppressed exciton-phonon coupling and increased intermolecular energy transfer, both of which are modulated by mechanical pressure. We first measured the pressure dependence of the vibrational modes. Raman spectroscopy reveals two phonon modes at 19 and 42  $cm^{-1}$  in silicone oil at 0.1 GPa, hereafter denoted as  $P_1$  and  $P_2$  respectively (Figure 2a). The same modes are observed at 22 and 47  $cm^{-1}$  in neon at 0.2 GPa (Figure 2b). Using density-functional perturbation theory (DFPT),<sup>[29]</sup> we show that  $P_1$  and  $P_2$  involve rotation and twisting of the  $H_4TBAPy$  monomers around the short and long axes of the pyrene, respectively, with the carboxylic hydrogens pinned at their lattice positions (left, Figure 2c,d). Further analysis shows that  $P_1$  consists of rotation and out-of-plane rocking of the phenyl side groups; both motions involve large changes in the dihedral angles between the pyrene and phenyl planes (right, Figure 2c; see also Figure S4 and Table S2, Supporting Information). This mode is known to vibronically couple to the electronically excited states in polyaromatic molecules, leading to non-radiative decay;<sup>[2,11,30,31]</sup> its suppression, therefore, is an origin of AIE through the so-called restriction of intramolecular motion (RIM) mechanism.<sup>[32]</sup> The eigenvector of  $P_2$  has a large projection on the direction perpendicular to the pyrene plane

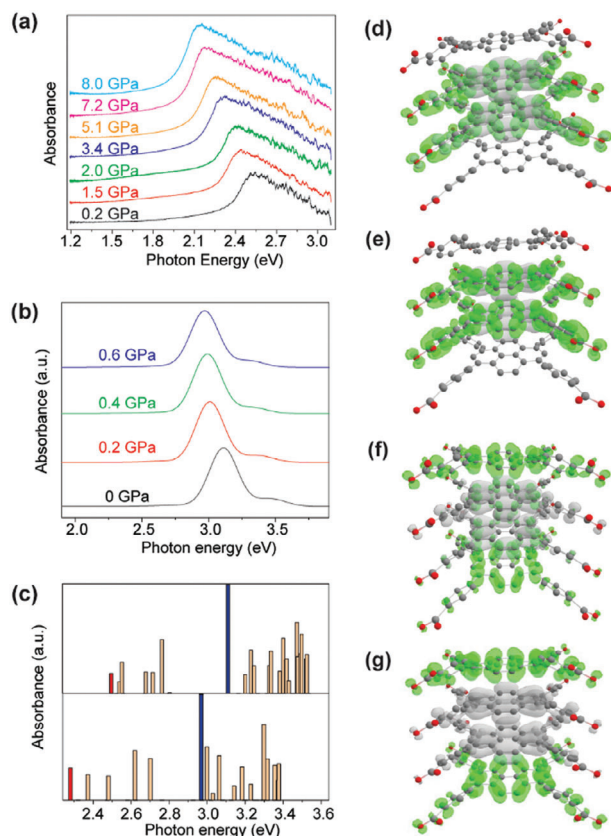


**Figure 4.** a) In situ pressure-dependent electronic absorption spectra of PFC-1. b) TD-DFT calculated the electronic absorption spectra of PFC-1 at different pressures. c) Oscillator strengths of first 20 electronic excited states from TD-DFT for (up) 0 GPa and (bottom) 0.6 GPa. The red-marked states indicate the lowest energy intermolecular charge-transfer transition (CT) and the blue states indicate the intramolecular excitations. EDDM of intramolecular excitation at d) 0 GPa and e) 0.6 GPa, isovalue = 0.02. EDDM of intermolecular CT at f) 0 GPa and g) 0.6 GPa, isovalue = 0.02.

(right, Figure 2d; see also Figure S4 and Table S2, Supporting Information); its frequency and intensity therefore serve as an indicator of the  $\pi$ - $\pi$  interaction strength.  $\pi$ - $\pi$  stacking facilitates intermolecular energy transfer, giving rise to ACQ in polyaromatic fluorophores.<sup>[7,33]</sup> DFPT calculation also identifies another phonon mode,  $P_3$ , which is energetically degenerate with  $P_2$ .  $P_3$  involves the rotation and twisting of the  $H_4TBAPy$  parallel to the pyrene plane (Figure S4, Supporting Information). While  $P_3$  is Raman active by symmetry, we expect it has little contribution to the observed Raman spectrum, as the associated motion does not induce the significant change of polarizability.

In silicone oil, both  $P_1$  and  $P_2$  blueshift with pressure in the range of 0–4 GPa (Figure 2e), with  $P_2$  showing a larger extent of change ( $33.9\text{ cm}^{-1}$ ) than  $P_1$  ( $8.7\text{ cm}^{-1}$ ). Their intensities diminish with increasing pressure, and  $P_2$  vanishes above 3 GPa. These observations indicate that pressure simultaneously suppresses the intramolecular vibration and enhances the intermolecular  $\pi$ - $\pi$  interaction. In the low-pressure range (0–2.1 GPa), suppression of the vibronic coupling dominates, manifested as pressure-induced PL enhancement. After 2.1 GPa, the contribution from intermolecular  $\pi$ - $\pi$  stacking becomes nontrivial, resulting in

competition between AIE and ACQ, and manifested as fluctuation of the PL intensity. Pressure-induced ACQ eventually dominates over AIE, leading to a prominent decrease of PL above 2.1 GPa. These results provide the first direct observation of the competition between, and tunability of, AIE and ACQ under pressure.

### 2.3. Effect of Guest Molecules

The PL and Raman spectra of PFC-1 in neon show similar yet more complicated behaviors (Figure 2f). The PL intensity fluctuates between 0 and 3 GPa. The AIE-ACQ crossover is delayed to higher pressure (3 GPa, c.f.  $\approx 2.1$  GPa in silicone oil).  $P_1$  and  $P_2$  blueshift by  $4.49$  and  $19.1\text{ cm}^{-1}$  from 0 to 3 GPa, respectively, much smaller than those observed in silicone oil.  $P_2$  intensity, although decreasing with pressure, nonetheless persists beyond 3 GPa. We attribute the difference between silicone oil and neon PTMs to their interaction with PFC-1. Both neon and silicone oil, that is, oligomeric poly(dimethylsiloxane), are small enough to enter the pores of PFC-1; however, neon may also penetrate the interstitial space between adjacent pyrenes, thereby weakening the intermolecular interaction and disrupting the  $\pi$ - $\pi$  stacking, leading to delayed onset of ACQ compared to the silicone oil.

### 2.4. DFT Modelling

To gain further insight into the structural changes as a function of pressure, we model the high-pressure structures of PFC-1 by density functional theory (DFT) using the Perdew–Burke–Ernzerhof (PBE) functional<sup>[34]</sup> and plane-wave basis sets.<sup>[35]</sup> The DFT-calculated structures show an expected decrease in the unit cell volume from 0 GPa to 0.6 GPa (Figure 3a; Figure S5 and Table S1, Supporting Information). The pore size decreases accordingly from 258 to 202 Å<sup>2</sup>. The unit cell is also slightly distorted, reflected by the change of lattice parameter  $\gamma$  from 93.64° at 0.2 GPa to 99.23° at 0.6 GPa (Figure 3a; Table S1, Supporting Information). The average dihedral angle between the pyrene and phenyl side groups decreases from 42.3° at 0 GPa to 38.7° at 0.6 GPa (Figure 3b,e), indicating increased coplanarity and more extended  $\pi$ -conjugation at high pressure. Interestingly, the  $c$ -axis (direction of stacking) shows slight expansion, from 3.77 Å at 0 GPa to 3.83 Å at 0.6 GPa (Figure 3c). Further analysis shows that the pyrene-pyrene distance perpendicular to the plane decreases slightly (from 3.53 Å at 0 GPa to 3.52 Å at 0.6 GPa), while the distance parallel to the plane increases with pressure (from 1.37 Å at 0 GPa to 1.49 Å at 0.6 GPa) (Figure 3d,f); that is, pressure drives a shear motion of the adjacent  $H_4TBAPy$  molecules. Such shearing behavior of molecular crystals under hydrostatic pressure has been observed in coordination polymer systems.<sup>[36]</sup> These findings suggest that the enhanced  $\pi$ - $\pi$  interaction mainly originates from enhanced coplanarity of the  $H_4TBAPy$  molecules, instead of compressed intermolecular distance. Indeed, the parallel motion depicted in the model might be expected to result in decreased  $\pi$ - $\pi$  interaction though the opposing contribution of the slight perpendicular compression is difficult to quantify. Above 0.6 GPa, the structure exhibits significant distortion, and the pores collapse (Figure S6, Supporting Information). Note that the DFT calculations assume a vacuum

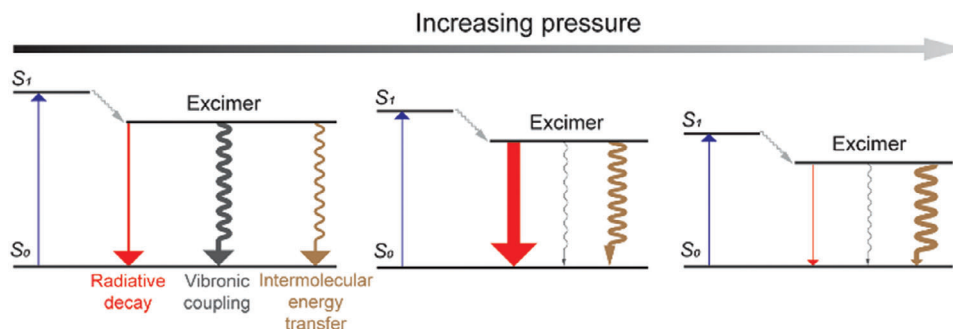


**Figure 5.** Jablonski diagram of pressure-modulated radiative versus nonradiative decay. The probability of each decay pathway is represented by the thickness of the line.

in the pore, while in experiments they are filled with PTM. Filling of the pores is known to provide additional support of the framework structure, retaining the porosity at higher pressure.<sup>[37]</sup>

### 2.5. Pressure-Dependent Optical Absorption

The optical absorption peak of PFC-1 shows a consistent redshift from 2.55 eV at 0.2 GPa to 2.14 eV at 8.0 GPa, indicating a diminished optical bandgap with increasing pressure (Figure 4a). To identify the intra- and inter-molecular contributions to the excited states, time-dependent density functional theory (TD-DFT) calculations are performed at the B3LYP/6-31G level on tetramer

of H<sub>4</sub>TBAPy stacked along the *c*-axis. The simulated absorption spectra faithfully reproduce the redshift with increasing pressure (Figure 4b). At both 0 and 0.6 GPa, the main absorption band (blue, Figure 4c) corresponds to the intramolecular charge-transfer from the pyrene to the phenyl arms, as revealed by the electron density difference maps (EDDMs, Figure 4d,e). Interestingly, an intermolecular excitation (Figure 4f,g) mode can be observed at lower energy (2.5 eV) at 0.2 GPa; EDDM indicates the corresponding charge-transfer to occur between adjacent pyrenes during the compression. (Figure S7, Supporting Information) This mode redshifts and gains intensity at 0.6 GPa, consistent with the pressure-enhanced  $\pi$ - $\pi$  interaction.

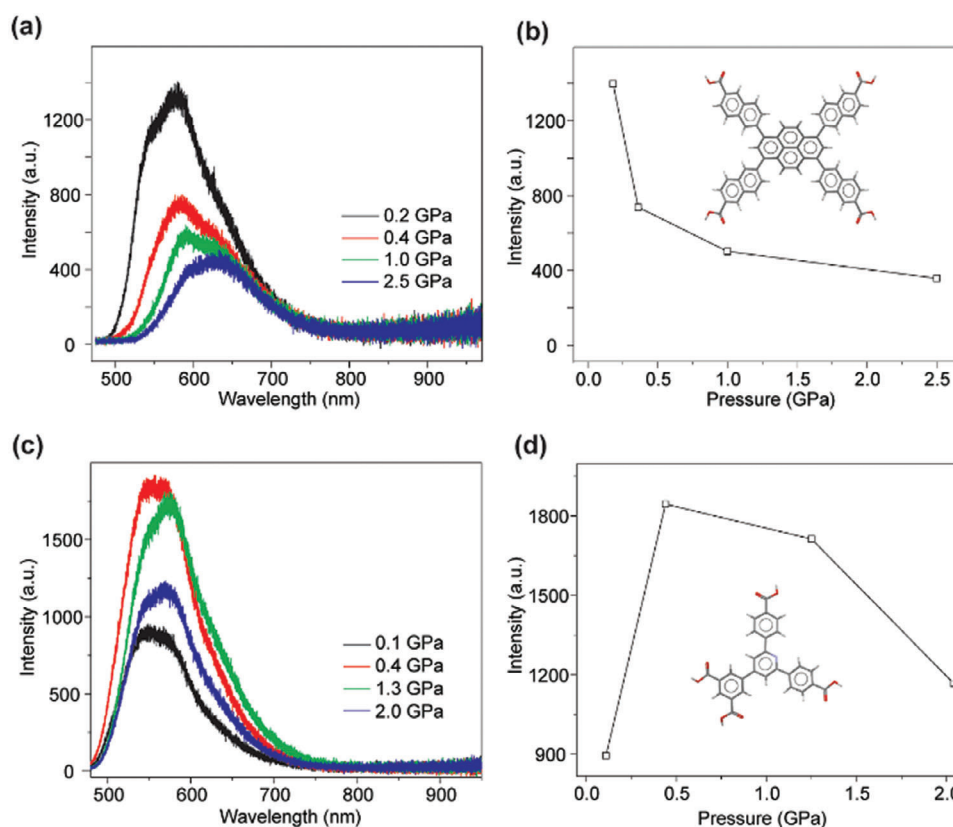


**Figure 6.** a) Pressure-dependent PL of HOF-14 and b) PL intensity function of pressure. The inset shows the structure of the monomer. c) Pressure-dependent PL of HOF-20. d) PL intensity function of pressure. The inset shows the structure of the monomer.

The photophysics involved in the pressure-modulated PL of PFC-1 is summarized in the Jablonski diagram shown in **Figure 5**. Photoexcitation initially populates the monomeric singlet state  $S_1$ , which quickly relaxes to the excimer state. The excimer then relaxes to the ground state through competing radiative and nonradiative pathways. Pressure initially enhances the radiative decay by suppressing the intramolecular vibronic coupling-induced quenching; however, as pressure further increases, intermolecular energy transfer dominates due to enhanced  $\pi$ - $\pi$  interactions,<sup>[38]</sup> leading to diminished PL.

## 2.6. Pressure-Modulated PL in HOF-14 and HOF-20

The rich reticular chemistry of HOFs allows us to test the pressure-modulated AIE-ACQ competition in a variety of structures with different chemical compositions and topologies. We first investigate the pressure-dependent PL of HOF-14 (**Figure 6a,b**), which is isoreticular to PFC-1. The monomer, 6,6',6'',6'''-(pyrene-1,3,6,8-tetrayl)tetrakis(2-naphthoic acid) (PT-TNA), consists of a pyrene core with four naphthoic acid side groups. In contrast to PFC-1, the PL intensity of HOF-14 shows a monotonic decrease from 0.2 to 2.5 GPa, indicating that pressure-enhanced ACQ dominates the emission. We attribute this to the larger conjugation system of HOF-14, which favors stronger  $\pi$ - $\pi$  interaction between stacked monomers. Pressure modulation of PL can also be extended to 3D HOFs, as demonstrated in the case of HOF-20 with pcu topology. The PL intensity of a HOF-20 single-crystal increases to 206.6% from 0.1 to 0.4 GPa, before dropping to 136.4% at 2.0 GPa (**Figure 6c,d**). These examples show that mechanically stable reticular materials may provide a versatile platform to study the photophysics of aggregated molecular systems, as well as for the discovery of functional materials.

## 3. Conclusion

In summary, In situ high-pressure spectroscopy of a porous HOF allowed, for the first time, direct observation of competition between AIE and ACQ in a fully reversible system. We show that even the presence of inert interstitial molecules within the pores and layers of our model system, PFC-1, tunes the pressure-response of this competition, increasing the maximum quantum yield by a factor of 25%. These findings also establish a correlation between low-frequency phonon modes and fluorescence intensity. The consequences of these findings are expected to have significant roles in many areas beyond piezo-luminescence, including the development of solid-state organic semiconductors for a multitude of technological applications.

## Supporting Information

Supporting Information is available from the Wiley Online Library or from the author.

## Acknowledgements

S.W. and P.E.V. contributed equally to this work. This research used resources of the National Synchrotron Light Source II; a U.S. Department of

Energy (DOE) Office of Science User Facility operated for the DOE Office of Science by Brookhaven National Laboratory under Contract No. DE-SC0012704. Use of the 22-IR-1 beamline is supported by the National Science Foundation Division of Earth Sciences (EAR) SEES: Synchrotron Earth and Environmental Science (EAR-2223273) and Chicago/DOE Alliance Center (CDAC) DE-NA0003975. Part of this work was performed on Crutch, the high-performance computing cluster at the University of North Texas supported by the NSF-MRI grants CHE-1531468 and OAC-2117247. This work was performed in part at the University of North Texas's Materials Research Facility: A shared research facility for multi-dimensional fabrication and characterization. Partial support from the Robert A Welch Foundation (B-0027) is also acknowledged (S.M.) and the Researchers Supporting Program (RSP2025R79) at King Saud University, Riyadh, Saudi Arabia (A.N.).

## Conflict of Interest

The authors declare no conflict of interest.

## Data Availability Statement

The data that support the findings of this study are available from the corresponding author upon reasonable request.

## Keywords

density-functional theory, diamond anvil cell, Raman spectroscopy, solid-state fluorescence

Received: November 26, 2024  
Revised: January 17, 2025  
Published online: February 3, 2025

- [1] C. Xu, R. Ye, H. Shen, J. W. Y. Lam, Z. Zhao, B. Z. Tang, *Angew. Chem., Int. Ed.* **2022**, *61*, 202204604.
- [2] Z. Zhao, H. Zhang, J. W. Y. Lam, B. Z. Tang, *Angew. Chem., Int. Ed.* **2020**, *59*, 9888.
- [3] Q. Li, Z. Li, *Adv. Sci.* **2017**, *4*, 1600484.
- [4] M. Fakis, D. Anastopoulos, V. Giannetas, P. Persephonis, *J. Phys. Chem. B* **2006**, *110*, 24897.
- [5] A. Y. Sosorev, O. D. Parashchuk, S. A. Zapunidi, G. S. Kashtanov, I. V. Golovnin, S. Kommanaboyina, I. F. Perepichka, D. Y. Parashchuk, *Phys. Chem. Chem. Phys.* **2016**, *18*, 4684.
- [6] Y. Dong, B. Xu, J. Zhang, X. Tan, L. Wang, J. Chen, H. Lv, S. Wen, B. Li, L. Ye, B. Zou, W. Tian, *Angew. Chem., Int. Ed.* **2012**, *51*, 10782.
- [7] Y. Huang, J. Xing, Q. Gong, L. C. Chen, G. Liu, C. Yao, Z. Wang, H. L. Zhang, Z. Chen, Q. Zhang, *Nat. Commun.* **2019**, *10*, 169.
- [8] S. R. Amrutha, M. Jayakannan, *J. Phys. Chem. B* **2008**, *112*, 1119.
- [9] J. Ren, L. Stagi, P. Innocenzi, *Prog. Solid State Chem.* **2021**, *62*, 100295.
- [10] J. Mei, N. L. C. Leung, R. T. K. Kwok, J. W. Y. Lam, B. Z. Tang, *Chem. Rev.* **2015**, *115*, 11718.
- [11] J. Luo, Z. Xie, J. W. Y. Lam, L. Cheng, H. Chen, C. Qiu, H. S. Kwok, X. Zhan, Y. Liu, D. Zhu, B. Z. Tang, *Chem. Commun.* **2001**, 1740.
- [12] H. Yuan, K. Wang, K. Yang, B. Liu, B. Zou, *J. Phys. Chem. Lett.* **2014**, *5*, 2968.
- [13] Z. Zhao, C. Chen, W. Wu, F. Wang, L. Du, X. Zhang, Y. Xiong, X. He, Y. Cai, R. T. K. Kwok, J. W. Y. Lam, X. Gao, P. Sun, D. L. Phillips, B. Z. Tang, *Nat. Commun.* **2019**, *10*, 768.
- [14] L. Ma, X. Feng, S. Wang, B. Wang, *Chem. Front.* **2017**, *1*, 2474.
- [15] Z. Ye, W. He, Z. Zhang, Z. Qiu, Z. Zhao, B. Z. Tang, *Interdiscip. Med.* **2023**, *1*, 20220011.

- [16] L. Dou, Q. Li, Z. Wang, J. Shen, W. Yu, *ACS Sens.* **2022**, *7*, 3243.
- [17] M. Asad, M. I. Anwar, A. Abbas, A. Younas, S. Hussain, R. Gao, L. K. Li, M. Shahid, S. Khan, *Coord. Chem. Rev.* **2022**, *463*, 214539.
- [18] L. L. Yang, H. Wang, J. Zhang, B. Wu, Q. Li, J. Y. Chen, A. L. Tang, J. W. Y. Lam, Z. Zhao, S. Yang, B. Z. Tang, *Nat. Commun.* **2024**, *15*, 999.
- [19] Y. Gu, K. Wang, Y. Dai, G. Xiao, Y. Ma, Y. Qiao, B. Zou, *J. Phys. Chem. Lett.* **2017**, *8*, 4191.
- [20] J. Fang, Z. Fu, X. Chen, Y. Liu, F. Chen, Y. Wang, H. Li, Y. Yusran, K. Wang, V. Valtchev, S. Qiu, B. Zou, Q. Fang, *Angew. Chem., Int. Ed.* **2023**, *62*, 202304234.
- [21] Q. Yin, P. Zhao, R. J. Sa, G. C. Chen, J. Lü, T. F. Liu, R. Cao, *Angew. Chem., Int. Ed.* **2018**, *57*, 7691.
- [22] E. Jin, M. Asada, Q. Xu, S. Dalapati, M. A. Addicoat, M. A. Brady, H. Xu, T. Nakamura, T. Heine, Q. Chen, D. Jiang, *Science* **2017**, *357*, 673.
- [23] K. Zhang, J. Liu, Y. Zhang, J. Fan, C. K. Wang, L. Lin, *J. Phys. Chem. C* **2019**, *123*, 24705.
- [24] M. Dharmawardana, B. M. Otten, M. M. Ghimire, B. S. Arimilli, C. M. Williams, S. Boateng, Z. Lu, G. T. McCandless, J. J. Gassensmith, M. A. Omary, *Proc. Nat. Acad. Sci.* **2021**, *118*, 2106572118.
- [25] J. Hao, M. Wang, S. Wang, Y. Huang, D. Cao, *Dyes Pigm.* **2020**, *175*, 108131.
- [26] W. Zhang, H. Xu, P. Shen, W. Zhang, G. Bai, S. Xu, *J. Solid State Chem.* **2024**, *337*, 124789.
- [27] B. Manna, D. K. Palit, *J. Phys. Chem. C* **2020**, *124*, 24470.
- [28] P. Deria, J. Yu, T. Smith, R. P. Balaraman, *J. Am. Chem. Soc.* **2017**, *139*, 5973.
- [29] P. Koskinen, V. Mäkinen, *Comput. Mater. Sci.* **2009**, *47*, 237.
- [30] R. Hu, A. Qin, B. Z. Tang, *Prog. Polym. Sci.* **2020**, *100*, 101176.
- [31] Y. Hong, J. W. Y. Lam, B. Z. Tang, *Chem. Commun.* **2009**, *29*, 4332.
- [32] N. L. C. Leung, N. Xie, W. Yuan, Y. Liu, Q. Wu, Q. Peng, Q. Miao, J. W. Y. Lam, B. Z. Tang, *Chem. - Eur. J.* **2014**, *20*, 15349.
- [33] Y. Cai, X. Ji, Y. Zhang, C. Liu, Z. Zhang, Y. Lv, X. Dong, H. He, J. Qi, Y. Lu, D. Ouyang, W. Zhao, W. Wu, *Aggregate* **2023**, *4*, e277.
- [34] Q. Zhang, M. Dai, H. Shao, Z. Tian, Y. Lin, L. Chen, X. C. Zeng, *ACS Appl. Mater. Interfaces* **2018**, *10*, 43595.
- [35] P. J. Hasnip, K. Refson, M. I. J. Probert, J. R. Yates, S. J. Clark, C. J. Pickard, *Phil. Trans. R. Soc. A* **2014**, *372*, 20130270.
- [36] H. Yan, F. Yang, D. Pan, Y. Lin, J. N. Hohman, D. SolisIbarra, H. Li, J. E. P. Dahl, M. K. Carlson, B. A. Tkachenko, A. A. Fokin, P. R. Schreiner, G. Galli, W. L. Mao, Z. X. Shen, N. A. Melosh, *Nature* **2018**, *554*, 505.
- [37] G. P. Robertson, S. Mosca, C. CastilloBlas, F. A. Son, O. K. Farha, D. A. Keen, S. Anzellini, T. D. Bennett, *Inorg. Chem.* **2023**, *62*, 10092.
- [38] G. Wang, B. Z. Tang, X. Gu, *Acc. Chem. Res.* **2024**, *57*, 1360.